Numerical Analysis of the Effects of Selected Geometrical Parameters and Fluid Properties on MHD Natural Convection Flow in an Inclined Elliptic Porous Enclosure with Localized Heating

T. Adekeye,[1,2] I. K. Adegun,[3] P. O. Okekunle,[2] A. K. Hussein,[4] S. O. Oyedepo,[1] E. Adetiba,[5] and O.S. I. Fayomi[1,6]

[1]Department of Mechanical Engineering, Covenant University, Ota, Ogun State, Nigeria

[2]Department of Mechanical Engineering, Ladoke Akintola University of Technology, Ogbomoso, Oyo State, Nigeria

[3]Department of Mechanical Engineering, University of Ilorin, Kwara State, Nigeria

[4]Department of Mechanical Engineering, College of Engineering, Babylon University, Babylon City, Iraq

[5]Department of Electrical, Information and Electronic Engineering, Covenant University, Ota, Ogun State, Nigeria

[6]Department of Chemical, Metallurgical & Materials Engineering, Tshwane University of Technology. Pretoria, South Africa

Magnetohydrodynamic (MHD) natural convection flow and associated heat convection in an oriented elliptic enclosure has been investigated with numerical simulations. A magnetic field was applied to the cylindrical wall of the configuration, the top and bottom walls of the enclosure were circumferentially cooled and heated, respectively, while the extreme ends along the cross-section of the elliptic duct were considered adiabatic. The full governing equations in terms of continuity, momentum, and energy transport were transformed into nondimensional form and solved numerically using finite difference method adopting Gauss–Seidel iteration technique. The selected geometrical parameters and flow properties considered for the study were eccentricity (0, 0.2, 0.4, 0.6, and 0.8), angle of inclination (0°, 30°, 60°, and 90°), Hartmann number (0, 25, and 50), Grashof number (10^4, 10^5, and 10^6), and Darcy number (10^{-3}, 10^{-4}, and 10^{-5}). The Prandtl number was held constant at 0.7. Numerical results were presented by velocity distributions as well as heat transfer characteristics in terms of local and average Nusselt numbers (i.e., rate of heat transfer). The optimum heat transfer rate was attained at e value of 0.8. Also, the heat transfer rate increased significantly between the angles of inclination 58° and 90°. In addition, Hartmann number increased with decreased heat transfer rate and flow circulation. A strong flow circulation (in terms of velocity distribution) was observed with increased Grashof and Darcy numbers. The combination of the geometric and fluid properties therefore can be used to regulate the circulation and heat transfer characteristics of the flow in the enclosure. © 2016 Wiley Periodicals,

© 2016 Wiley Periodicals, Inc.

Inc. Heat Trans Asian Res, 46(3): 261–293, 2017; Published online in Wiley Online Library (wileyonlinelibrary.com/journal/htj). DOI 10.1002/htj.21211

Key words: MHD, natural convection, inclined elliptic enclosure, porous media, localized heating

Highlights

- Numerical simulation of the effects of selected geometrical and fluid properties on MHD natural convection in an inclined elliptic porous enclosure.
- Finite difference method adopting Gauss–Seidel iteration techniques is used to solve this problem.
- Average Nusselt Number (Nu_a) for the parametric range $0.6 \leq e < 1$ is mixed convection conduction.
- Local Nusselt number (Nu) increased for the parametric range $0.4 \leq e < 1$, that is, 0.4 to 0.8.
- Inclination angle increases significantly for the range $58° \leq \emptyset \leq 90°$, that is, 58° and 90° inclination.
- Hartmann number effect increasing with decreasing flow circulation (i.e., velocity distribution). Grashof and Darcy numbers effect increasing strongly with increasing flow circulation (velocity distribution) for Grashof number = 10^6 and 10^{-4}.

1. Introduction

One of the most important phenomenon in a thermal system is free or natural convection, this is due to its wide applications in nature and engineering such as oceanic current, sea-wind, fluid flows around shrouded heat dissipation fins, free air cooling without the aid of fans, electronic cooling, heat exchanger between the soil and atmosphere, high performance insulation for buildings, chemical catalytic reactors, food processing, electrochemistry, metallurgy, grain storage, cooling of radioactive waste containers, solar collector energy, and compacted bed for the chemical industry to mention a few [1, 2]

So far, many studies in the field of natural convection inside simple enclosures have been performed so that it is a classic problem now. However, the natural convection heat transfer problem inside an enclosure with a nonsimple shape and with different geometry is a topic that has recently received more attention. Based on the published papers in the field, it can be claimed that the subject has been seriously investigated with the development of numerical methods and related hardware in the past two decades [3].

In the same vein, natural convection heat transfer inside irregular and complex shaped enclosures has a wide variety of technology or engineering applications. This is because various geometries have been receiving a growing interest recently due to their potential engineering applications in electronic package, electronic equipment, solar power receivers, grain storage, and so on. In fact, actual enclosures occurring in practice often have a geometry different from a rectangular shape [4].The research of natural convection in porous media has been conducted widely in recent years, which involves post-accidental heat removal in nuclear reactors, cooling and radioactive waste, energy efficiency, drying processes, to mention a few [4].

Also, magnetohydrodynamic (MHD) flows, which are the simplest plasma model, have been the subject of a great number of empirical and theoretical investigations in physics. Most especially, the MHD flow associated with heat transfer has received considerable attention so far, as their application resides in many industrial fields, such as an MHD generator that transforms thermal and kinetic energy directly into electrical energy by eliminating the boiler and turbine due to high operating temperature, electric propulsions for space exploration, crystal growth in liquids, cooling of nuclear reactors, microelectronic devices, electronic packages, geothermal energy extraction, boundary layer control in the field of aerodynamic, electromagnetic casting and control mechanism in material manufacturing industries among others [5, 6].

In addition, in industry, the quality of a crystal is affected adversely by instabilities in the melt phase because instabilities impose temperature fluctuations at the solidification front and leads to striations in the crystalline product. It is well known that applying a magnetic field to the system leads to damping unavoidable hydrodynamic movement and consequently growing high quality crystals. In general, the quality and homogeneity of single crystals growth from dripped semiconductor melts are very important and interesting for the manufacture of semi and super conductors [7]. Some other quite promising applications are pertinent to metallurgy, such as MHD stirring of molten metal and magnetic levitation casting. In such cases, an electrically conducting fluid becomes involved in a magnetic field [8].

Though many studies have begun to appear in the literature which deal with natural convection heat transfer with or without porous media for non-rectangular enclosure shapes such as triangular, L-shaped, trapezoid, elliptical, wavy, rhombic, parallelogram-shaped enclosures and so on. Special attention is given to elliptic enclosures because of their increasing heat transfer coefficient, reduction in the rate of heat transfer losses, creation of less resistance to the cooling fluid, which results in less pumping power in the case of forced flow and in the case of power failure for the case of natural convection. An elliptic geometry is flexible enough to approach a circular tube when the axis ratio approaches unity and approaches a flat plate when the axis ratio becomes very small [9, 10]. Mota and colleagues [11] investigated numerically natural convection in horizontal eccentric elliptic annuli containing saturated porous media. Governing equations were solved in a generalized orthogonal coordinate system using high-order compact finite difference method. Effects of geometrical parameters such as eccentricity, ratio axis length of elliptic enclosure as well as cylinder were investigated on heat transfer rate at a constant Ra = 100 and hydraulic-radius ratio (2). They concluded that the rate of heat transfer losses could be minimized by a proper choice of the elliptic shape of a concentric annulus which could be further enhanced if the geometry was made eccentric.

The use of ducts with an elliptic cross-section has increased in modern engineering heat transfer applications such as compact heat exchanger, flow passage and so on. Kakac and colleagues [12] reported that the main advantage of using elliptic ducts over circular ducts was the increasing heat transfer coefficient with the elliptic-shaped duct. Eid [13] investigated natural convection heat transfer in elliptical annuli with different aspect ratio experimentally and numerically. The study showed that natural convective heat transfer in concentric elliptic annuli increased by about 40% more than the circular annuli having the same perimeter. Sakalis and colleagues [14] reported laminar, incompressible hydrodynamically fully developed flows in straight elliptical ducts with the aspect ratio varying from 0.25 to 0.99. The duct wall was subjected successively to constant temperature, circumferentially uniform and axially linearly varying temperature. Numerical results

obtained with an ADI scheme (alternating direction implicit) indicated that the friction factor increased as aspect ratio decreased and high Nusselt number decreased as aspect ratio decreased. Also, Nusselt numbers increased for small axial wall temperature distribution, which decreased for large axial wall temperature values. Abdel-Wahed and colleagues [15] carried out an extensive experimental investigation on laminar developing and fully developed flows and heat transfer in a horizontal elliptical duct. The result predicted that the optimum heat transfer rate for a tube occurred at eccentricity, e = 0.866. Mahfouz [16] studied numerically the buoyancy driven flow in an inclined elliptic enclosure using Fourier Spectra method. He concluded that the angle of inclination increased with the total rate of heat transfer for the case of a uniform wall temperature (UWT) while in case of uniform heat flux (UHF), the increased angle of inclination decreased the mean temperature of the inner wall of the enclosure. Ghasemi and colleagues [17] presented natural convection between a circular enclosure and an elliptical cylinder using a control volume-based finite element method. The result showed that the smaller the size of the elliptic cylinder, the more room for flow circulation and the higher the strength of the flow regime. Bello-Ochende and Adegun [18] reported a perturbation analysis of a combination of free and forced laminar convection in a tilted elliptic cylinder. They concluded that the heat transfer and fluid results for the range of eccentricity, $0 \leq e \leq 1$, showed that $e = 0.866$ the local Nusselt number exhibited significant dependence on the azimuthal angle. It also indicated that the optimal value of mean Nusselt number occurred when $e = 0.866$. Adegun and Oladosun [19] investigated a scale analysis of free and forced convection heat transfer in an elliptic conduit. The results obtained showed that the generalized Nusselt number was dependent solely on the eccentricity of the ellipse. It also indicated that the Nusselt number at the end of minor axis was greater than that of the major axis [20]. Fatih and Hakan numerically investigated MHD mixed convection in a nanofluid filled lid-driven square enclosure with a rotating cylinder using the finite element method. They concluded that the averaged heat transfer rate decreased with increased Hartmann number and 14.2% of the heat transfer enhancement was obtained for a rotating cylinder as compared to the stationary case. Also, they found that magnetic field application suppressed the velocity field flow and convection and in the same vein, it could be used to control the local Nusselt number since it acted to increase the rate of heat transfer toward the right end of the bottom wall of the configuration for the parametric range $0.35 \leq X \leq 0.75$ [21]. Fatih and Hakan numerically studied MHD mixed convection of a nanofluid filled partially heated triangular enclosure with a rotating adiabatic cylinder using Finite element method. They concluded that an increased Hartmann number decreased the total entropy generation, local and averaged Nusselt numbers. Also, they discovered that average Nusselt number increased with the Grashof number to heat enhancement of 231.1% for $\mathrm{Gr} = 10^6$ compared to the case at $\mathrm{Gr} = 10^4$. Again, they observed that angular rotational speed of the cylinder could be used as a control mechanism for flow and temperature distribution within the triangular enclosure, and in the same vein, they found that average heat transfer enhancements of 50.4% and 37.4% were obtained for a rotating cylinder compared to the motionless case [22]. Fatih and Hakan numerically considered natural convection in a nanofilled cavity having different shaped obstacles (circular, square, and diamond) installed under the influence of a uniform magnetic field and heat generation using Galerkin weighted residual finite element formulation. They found that the presence or application of the obstacles retarded the heat transfer process and became more pronounced with higher values of Raleigh numbers. The average heat transfer was reduced by 21.35%, 32.8%, and 34.64% for the cavity with circular, diamond, and square shaped obstacles compared to the case without obstacles. They also discovered that the topography and thermal patterns were affected by the application of a magnetic field, nanoparticles, and different shaped obstacles [23]. Fatih and Hakan investigated the influence of inclination angle

of the magnetic field on mixed convection of nanofluid flow over a backward facing step and entropy generation using finite element method. They concluded that the averaged heat transfer increased as the Reynolds number increased and the effect became enormous with higher values of inclination angle of the magnetic field. Also, they noticed that as the value of the Hartmann number decreased for a horizontal aligned magnetic field, the volume fraction of the nanoparticles increased the average and local Nusselt numbers. It was also discovered that for the inclined and vertical magnetic field, suppression of the recirculation behind the step was noticed as a result of the increased value of Hartmann number. Israel and Amos [24] investigated numerically MHD oscillatory coquette flow of a radiating viscous fluid in a porous medium with periodic wall temperature. They concluded that the flow velocity increased with an increased magnetic field, Grashof number and the porosity. Ahmed [25] used the finite volume method with a collocated grid to analyze the natural convection in a parabolic enclosure. The heat transfer rate analyzed with local and average Nusselt numbers for the bottom wall of the enclosure showed that the local heat transfer rate was larger for the small value of the parabolic equation constant (C = 0.1) and also average heat transfer rate was higher for the same constant value. Moghimi and colleagues [26] studied numerically natural convection in an inclined L-shaped porous enclosure using the finite difference method via Marker and Cell Approach (MAC). They concluded that decrement of Darcy number decreased the rate of heat transfer and inclination angle had an important effect on isotherms and streamlines at a high Rayleigh number. Habibis and colleagues [27] studied numerically natural convection flow in a parallelogramic region filled with an electrically conducting fluid in a fluid saturated medium. They concluded that the convection model within the enclosure was dependent on the Rayleigh number and inclination angle. Hakan and colleagues [28] studied numerically the effect of joule heating MHD natural convection in a nonisothermally heated enclosure. The results showed that the flow was weaker near the right corner of the cavity due to a nonisothermal boundary condition.

Focus of the Work

The present study is an investigation of the effect of salient geometric parameters and fluid properties on an electrically conducting fluid flow within an inclined elliptic porous enclosure subjected to localized heating. The authors used the finite difference method adopting the Gauss–Seidel iteration technique. A physical model of the problem is shown in Fig 1. The whole cross-section of an elliptic domain was used in the numerical computation. The duct walls required circumferentially cooled and heated regions A_1A_2 and B_1B_2 as well as major and minor diameters, “a” and “b,” respectively. For the discretization of the governing equations, the central difference quotients were used for the second-order derivatives. Algebraic equations obtained for each variable were solved by a simple form of the Gauss–Seidel iteration procedure because it generates a well-refined estimate of the solution and its error could be controlled by the number of iterations. A computer algorithm was developed to simulate the fluid flow and heat transfer in the enclosure.

Nomenclature

b: minor diameter of the enclosure
a: major diameter of the enclosure
Ar: aspect ratio
B_0: magnitude of the magnetic field, Tesla
C_p: specific heat at constant pressure J/kg °C
D_h: hydraulic diameter, m

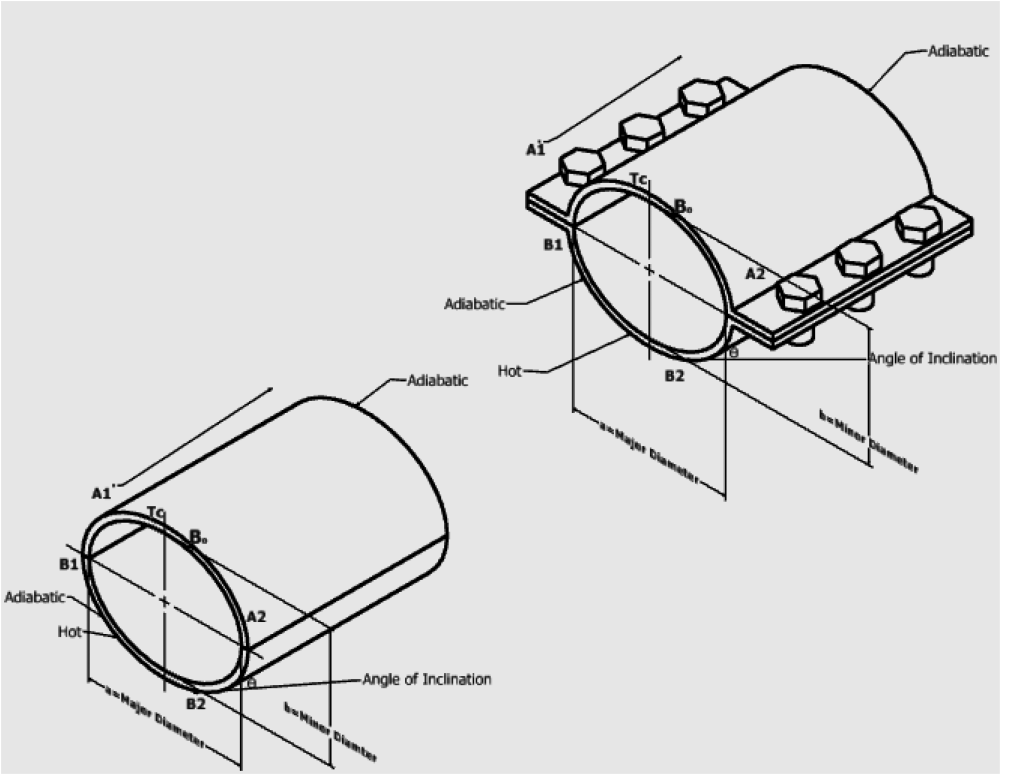

Fig. 1. Schematic diagram of the physical model of the problem. [Color figure can be viewed in the online issue, which is available at wileyonlinelibrary.com/journal/htj.]

g: gravitational acceleration, m/s^2
Ha: Hartmann number = $(\frac{B_0 a\sqrt{Q_e}}{\rho\nu})$
Da: Darcy number, (k/a^2)
Gr: Grashof number = $(\frac{g.\beta.\Delta T a^3}{\nu^2})$
Pr: Prandtl number = $(\frac{\nu}{\alpha})$
U_R: dimensionless velocity component in radial direction
$\mathbf{U}_{\emptyset}$: dimensionless velocity component in Azimuthal direction
k: thermal conductivity, W/m °C
K: permeability of the saturated porous medial,m^2
P: dimensionless pressure
p: pressure, N/m^2
NU: local Nusselt number
NU_a: average Nusselt number
q: heat flux, W/m^2
RR: radial direction
r: dimensional radius
R: dimensionless radius
t: dimensional temperature
T: dimensionless temperature

Greek Symbols

α: thermal diffusivity $= \frac{\mathbf{m}^2}{\mathbf{s}}$
β: volumetric thermal expansion coefficient, K^{-1}
φ: dimensionless stream function
Δ: dimensionless heat generation or absorption parameter
e: dimensionless ellipse, eccentricity $= (\sqrt{1 - Ar^2})$
Θ: enclosure inclination angle, °C
$\emptyset$: azimuthal angle
v: fluid kinematic viscosity, $\frac{\mathrm{m}^2}{\mathrm{s}}$
p: fluid density, $\frac{\mathrm{kg}}{\mathrm{m}^3}$
$\boldsymbol{\sigma_e}$: fluid electrical conductivity, W/m °C

Abbreviation

MHD: magnetohydrodynamics
Eq.: equation
CFD: computational fluid dynamics

2. Mathematical Modeling

This section presents the physical model of an inclined elliptic enclosure with localized heating. Governing equations of continuity, momentum, and energy transport were nondimensionalized using some heat transfer indices. The resulting nonlinear system of partial differential equations were solved using the finite difference method adopting the Gauss–Seidel iteration technique.

The MHD natural convection flow of an elliptic enclosure of major diameter, a, and minor diameter, b, filled with a fluid saturated porous medium is considered as shown in Fig. 1 along with the important geometry parameters. The top $\overline{A_1 A_2}$ and bottom $\overline{B_1 B_2}$ walls are simultaneously cooled and heated, respectively, and the two extreme ends along the cross-section of the elliptic ducts are considered adiabatic. An external magnetic field of magnitude (B_0) is applied on the cylindrical wall of the enclosure and at an angle θ to the inclined side wall. The Hartmann number is varied as $0 \leq Ha \leq 50$, the Darcy number is taken as Da$\leq 10^{-3}, 10^{-4}$, and 10^{-5}, the Grashof number is varied as $10^4 \leq Gr \leq 10^6$ to cover both buoyancy and magnetic field dominant flow regimes, the Prandtl number is held constant at Pr = 0.7, eccentricity varied as 0, 0.2, 0.4, 0.6, and 0.8 while the elliptical enclosure inclination angle is varied as$0^0 \leq \theta \leq 90^0$, respectively. The specific boundary conditions for the enclosure at the elliptic wall with all relevant parameters considered in the domain are all included in the governing equations.

2.1 Basic assumptions

The following assumptions are made in the present work:

(i) The flow is assumed to be two dimensional (2D), that is, there is no flow in the axial direction.

(ii) Steady-state condition is also assumed, that is, $\frac{\partial U}{\partial t} = \frac{\partial V}{\partial t} = \frac{\partial T}{\partial t} = 0$.

(iii) Velocity components at the walls are zero, that is,$U_r = U_\emptyset = 0$, no slip boundary condition.

(iv) Gravity acts vertically downward.

(v) The axial heat fluxes in the fluid are negligible.

(vi) Viscous dissipation effects are considered to be negligible.

(vii) The working fluid is considered an electrically conducting Newtonian fluid.

(viii) Radiation and joule heating effects are negligible.

(ix) The flow is considered incompressible, that is, $\rho =$ constant.

2.2. Governing equations and geometrical configurations

2.2.1. The dimensional form of the governing equations

The governing equations are formulated based on the assumptions made in 2.1, the flow and thermal fields inside the elliptic enclosure are modeled by the Navier–Stokes and the energy equations, respectively, which are given in a primitive or dimensional form as follows, Verzicco and Orlandi [29]:

2.2.2. Continuity equation

The dimensional form of continuity governing equation is given as,

$$\frac{\partial U_r}{\partial r} + \frac{U_r}{r} + \frac{1}{r}.\frac{\partial U_\phi}{\partial \phi} = 0\,. \tag{1}$$

2.2.3. Radial direction (r)

The dimensional form of momentum governing equation in the radial direction is given as

$$A = B + C - D, \tag{2a}$$

where

$$A = \rho\left[\frac{\partial U_r}{\partial t} + \frac{U_r \partial U_r}{\partial r} + \frac{U_\phi}{r}.\frac{\partial U_r}{\partial \phi} - \frac{{U_\phi}^2}{r}\right], \tag{2b}$$

$$B = \rho g \beta \left(t - t_{ref}\right)\cos\theta - \frac{\partial p}{\partial r}, \tag{2c}$$

$$C = \mu \left[\frac{\partial^2 U_r}{\partial r^2} + \frac{1}{r^2}.\frac{\partial^2 U_r}{\partial \phi^2} + \frac{1}{r}.\frac{\partial U_r}{\partial r} - \frac{2}{r^2}.\frac{\partial U_\phi}{\partial \phi} - \frac{U_r}{r^2} \right] - \frac{\rho \upsilon}{k} U_r, \tag{2d}$$

$$D = \sigma_e {B_0}^2 \upsilon. \tag{2e}$$

Dividing Eq. (2a) through by ρ, yields

$$Y = A + B - C, \tag{3a}$$

where

$$Y = \left[\frac{\partial U_r}{\partial t} + \frac{U_r \partial U_r}{\partial r} + \frac{U_\phi}{r}.\frac{\partial U_r}{\partial \phi} - \frac{{U_\phi}^2}{r} \right], \tag{3b}$$

$$A = g\beta \left(t - t_{ref} \right) \cos\theta - \frac{\partial p}{\rho \partial r}, \tag{3c}$$

$$B = \upsilon \left[\frac{\partial^2 U_r}{\partial r^2} + \frac{1}{r^2} \frac{\partial^2 U_r}{\partial \phi^2} + \frac{1}{r} \frac{\partial U_r}{\partial r} - \frac{2}{r^2}.\frac{\partial U_\phi}{\partial \phi} - \frac{U_r}{r^2} \right] - \frac{\upsilon}{k} U_r, \tag{3d}$$

$$C = \frac{\sigma_e {B_0}^2}{\rho} \upsilon. \tag{3e}$$

For a steady-state condition,

$$\frac{\partial u}{\partial t} = 0. \tag{3f}$$

Therefore, Eq. (3a) becomes

$$K = X + Y - Z, \tag{4a}$$

where

$$K = \frac{U_r \partial U_r}{\partial r} + \frac{U_\phi}{r}.\frac{\partial U_r}{\partial \phi} - \frac{{U_\phi}^2}{r}, \tag{4b}$$

$$X = g\beta \left(t - t_{ref} \right) \cos\theta - \frac{\partial p}{\rho \partial r}, \tag{4c}$$

$$Y = \upsilon \left[\frac{\partial^2 U_r}{\partial r^2} + \frac{1}{r^2} \frac{\partial^2 U_r}{\partial \phi^2} + \frac{1}{r} \frac{\partial U_r}{\partial r} - \frac{2}{r^2}.\frac{\partial U_\phi}{\partial \phi} - \frac{U_r}{r^2} \right] - \frac{\upsilon}{k} U_r, \tag{4d}$$

$$Z = \frac{\sigma_e {B_0}^2}{\rho} \upsilon. \tag{4e}$$

2.2.4. Azimuthal direction (ϕ)

The dimensional form of governing equation in the azimuthal direction is given as

$$Q = P + R - T, \tag{5a}$$

where

$$Q = \rho \left[\frac{\partial U_\phi}{\partial t} + \frac{U_r \partial U_\phi}{\partial r} + \frac{U_\phi}{r} \frac{\partial U_\phi}{\partial \phi} + \frac{U_r U_\phi}{r} \right], \tag{5b}$$

$$P = \rho g \beta \left(t_w - t_{ref}\right) \sin\theta - \frac{1}{r}\frac{\partial p}{\partial \phi}, \tag{5c}$$

$$R = \mu \left[\frac{\partial^2 U_\phi}{\partial r^2} + \frac{1}{r^2}\frac{\partial^2 U_\phi}{\partial \phi^2} + \frac{1}{r}\frac{\partial U_\phi}{\partial r} + \frac{2}{r^2}.\frac{\partial U_r}{\partial \phi} - \frac{U_\phi}{r^2} \right], \tag{5d}$$

$$T = \frac{\rho \upsilon}{k} U_\phi. \tag{5e}$$

Dividing Eq. (5a) through by ρ, yields

$$S = U + V - W, \tag{6a}$$

where

$$S = \left[\frac{\partial U_\phi}{\partial t} + \frac{U_r \partial U_\phi}{\partial r} + \frac{U_\phi}{r}\frac{\partial U_\phi}{\partial \phi} + \frac{U_r U_\phi}{r} \right], \tag{6b}$$

$$U = g\beta \left(t - t_{ref}\right) \sin\theta - \frac{1}{\rho r}\frac{\partial p}{\partial \phi}, \tag{6c}$$

$$V = \upsilon \left[\frac{\partial^2 U_\phi}{\partial r^2} + \frac{1}{r^2}\frac{\partial^2 U_\phi}{\partial \phi^2} + \frac{1}{r}\frac{\partial U_r}{\partial r} + \frac{2}{r^2}.\frac{\partial U_r}{\partial \phi} - \frac{U_\phi}{r^2} \right], \tag{6d}$$

$$W = \frac{\upsilon}{k} U_\phi. \tag{6e}$$

For a steady-state condition,

$$\frac{\partial U_\phi}{\partial t} = 0\,, \tag{6f}$$

$$F = G + H - I, \tag{7a}$$

where

$$F = \left[\frac{U_r \partial U_\phi}{\partial r} + \frac{U_\phi}{r}\frac{\partial U_\phi}{\partial \phi} + \frac{U_r U_\phi}{r} \right], \tag{7b}$$

$$G = g\beta \left(t - t_{ref}\right) \sin\theta - \frac{1}{\rho r}\frac{\partial p}{\partial \phi}, \tag{7c}$$

$$H = \upsilon \left[\frac{\partial^2 U_\phi}{\partial r^2} + \frac{1}{r^2}\frac{\partial^2 U_\phi}{\partial \phi^2} + \frac{1}{r}\frac{\partial U_r}{\partial r} + \frac{2}{r^2}.\frac{\partial U_r}{\partial \phi} - \frac{U_\phi}{r^2} \right], \tag{7d}$$

$$I = \frac{\upsilon}{k} U_\phi. \tag{7e}$$

2.2.5. Energy transport equation

The primitive energy transport governing equation is given as,

$$\frac{k\partial^2 t}{\partial r^2} + \frac{k}{r^2}.\frac{\partial^2 t}{\partial \phi^2} + \frac{k}{r}.\frac{\partial t}{\partial r} = \rho C_p \left[U_r \frac{\partial t}{\partial r} + U_\phi \frac{\partial t}{r \partial \phi} \right]. \tag{8}$$

2.3. Normalized boundary conditions

The dimensionless boundary conditions of the elliptic enclosure are expressed as follows:

$$U_r = U_\emptyset = 0\,. \tag{9}$$

The boundary condition along the walls of the elliptic duct is the no-slip condition and impermeability.

The upper circumferential elliptic wall of the enclosure is maintained at constant cold temperature (T_c) so that

$$U_r = U_\phi = T = 0. \tag{10}$$

The inclined lower circumferential elliptic wall of the enclosure is subjected to a constant heat flux,

$$\frac{\partial q}{\partial r} = 0. \tag{11}$$

The two extreme ends are considered adiabatic:

$$\frac{\partial T}{\partial r} = 0. \tag{12}$$

2.4. The normalized governing equations

It is regarded that the results of this study be valid for all physical model (within the scope of the study). It is therefore necessary to express the dimensional governing equations and the associated boundary conditions in the nondimensional form, so that the results thus obtained could be generalized for a wide variety of physical situations. Hence the following dimensionless quantities or transforming parameters are considered in the present work:

2.4.1. Transforming parameters

$$R = \frac{r}{a},\ \ U_R = \frac{u_r a}{\upsilon},\ \ U_\phi = \frac{u_\phi a}{\upsilon},\ \ P = \frac{p}{p_{ref}},\ \ T = \frac{t - t_{ref}}{\Delta t},\ \ \Delta T = \frac{qa}{k},$$

$$Pr = \frac{\upsilon}{\alpha} = \frac{\rho C_p \upsilon}{k}, Ra = \frac{g\beta\Delta T a^3}{\upsilon\alpha},\ \ Ha = \frac{B_0 a\sqrt{\sigma_e}}{\sqrt{\rho\upsilon}}, \mathrm{Gr} = \frac{g\beta\Delta T a^3}{\nu^2},$$

$$Da = \frac{k}{a^2}, \Delta = \frac{Q_0 a^2}{\rho\alpha C_p},\ \ U_R = \frac{1}{R}\frac{\partial\psi}{\partial\phi},\ \ U_\phi = -\frac{\partial\psi}{\partial R},\ \ R = \frac{r}{a} = \eta = \sqrt{\frac{1-e^2}{1-e^2\sin^2\phi}}.$$

2.4.2. Normalized continuity equation

$$\frac{\partial U_R}{\partial R} + \frac{U_R}{R} + \frac{\partial U_\emptyset}{R\partial\phi} = 0\ . \tag{13}$$

2.4.3. Normalized momentum equations

2.4.3.1. Radial direction

The normalized momentum equation in radial direction is given as

$$B = A - C - K, \tag{14a}$$

where

$$B = U_R \cdot \frac{\partial U_R}{\partial R} + \frac{U_\phi}{R} \cdot \frac{\partial U_R}{\partial \phi} - \frac{{U_\phi}^2}{R}, \tag{14b}$$

$$A = A = Gr \cos\theta, \tag{14c}$$

$$C = \left[\frac{\partial P}{\partial R} - \frac{\partial^2 U_R}{\partial R^2} - \frac{1}{R^2} \cdot \frac{\partial^2 U_R}{\partial \phi^2} - \frac{1}{R} \cdot \frac{\partial U_R}{\partial R}\right], \tag{14d}$$

$$K = \left[\frac{2}{R^2} \cdot \frac{\partial V}{\partial \phi} + \frac{U_R}{R^2} + \frac{U_R}{Da} + Ha^2\right]. \tag{14e}$$

2.4.3.2. Azimuthal direction

The normalized momentum equation in azimuthal direction is given as

$$B = A - L + D, \tag{15a}$$

where

$$B = \left[U_R \cdot \frac{\partial U_\emptyset}{\partial R} + \frac{U_\phi}{R} \cdot \frac{\partial U_\emptyset}{\partial \phi} + \frac{U_R U_\emptyset}{R}\right], \tag{15b}$$

$$A = Gr \ \sin\theta, \tag{15c}$$

$$L = \left[\frac{1}{R} \cdot \frac{\partial p}{\partial \phi} - \frac{\partial^2 U_\emptyset}{\partial R^2} - \frac{1}{R^2} \cdot \frac{\partial^2 U_\emptyset}{\partial \phi^2}\right], \tag{15d}$$

$$D = \left[\frac{\partial U_R}{\partial R} + \frac{2}{R^2} \cdot \frac{\partial U_R}{\partial \phi} - \frac{U_\phi}{R^2} - \frac{U_\phi}{Da}\right]. \tag{15e}$$

2.4.4. Normalized energy transport

The normalized energy transport governing equation is expressed below as

$$\frac{\partial^2 T}{\partial R^2} + \frac{1}{R^2} \cdot \frac{\partial^2 T}{\partial \phi^2} + \frac{1}{R} \cdot \frac{\partial T}{\partial R} = Pr \left[U_R \cdot \frac{\partial T}{\partial R} + \cdot U_\phi \frac{\partial T}{R \partial \phi}\right]. \tag{16}$$

2.5. Finite difference analogue (FDA) of the normalized governing equations (discretization)

Finite difference approximations replace functions by their corresponding difference quotients. Generally, the domain under consideration is divided into grids or meshes, which can be of any shape. Points of intersection of the mesh lines form the node, which serves as a point of evaluation.

The method is considered approximate in that the derivative at a given point is represented by a derivative taken over a finite interval across the point. However, the accuracy of such an approximation can be controlled by choosing the interval as small as possible at the expense of increased computational efforts resulting in increased number of algebraic equations. [30]

Considering the computational model for an elliptic domain in Fig. 1

(i) The duct wall requires "simultaneous cooled and heated regions $\overline{A_1 A_2}$" and "$\overline{B_1 B_2}$"

(ii) Major and minor diameters are a and b, respectively.

2.5.1. FDA of normalized continuity equation

The mathematical expression below shows the FDA for the continuity governing equation from Eq. (13) given as

$$\frac{\partial U_R}{\partial R} + \frac{U_R}{R} + \frac{1}{R} \cdot \frac{\partial U_\emptyset}{\partial \emptyset} = 0,$$

$$\frac{\partial U_R}{\partial R} = \frac{U_{Ri+1,j} - U_{i,j}}{\Delta R}, \tag{17a}$$

$$\frac{1}{R} = \frac{1}{R_{i,j}}, \tag{17b}$$

$$\frac{\partial U_\emptyset}{\partial \emptyset} = \frac{U_{\emptyset i,j+1} - U_{\emptyset i,j}}{\Delta \emptyset}, \tag{17c}$$

$$\frac{U_R}{R} = \frac{U_{Ri,j}}{R_{i,j}}. \tag{17d}$$

Substituting Eqs. (17a) to (17d) into Eq. (13), yields

$$U_{Ri,j} = \frac{U_{Ri+1,j} \cdot R_{i,j} + \left(U_{\emptyset i,j+1} - U_{\emptyset i,j}\right)\left(\frac{\Delta R}{\Delta \emptyset}\right)}{R_{i,j} - \Delta R}. \tag{17e}$$

Simplifying Eq. (17e) gives the discretized form of continuity equation

$$U_{Ri,j} = \frac{A_{i,j}\left(U_{Ri+1,j}\right) + C\left(U_{\emptyset i,j+1} - U_{\emptyset i,j}\right)}{D_{i,j}}, \tag{17f}$$

where

$$A_{i,j} = R_{i,j}, \tag{17g}$$

$$C = \Delta R / \Delta \emptyset, \tag{17h}$$

$$D_{i,j} = R_{i,j} - \Delta R. \tag{17i}$$

2.5.2. FDA of the normalized momentum equation

The mathematical expression below shows the FDA of normalized momentum governing equation in Eq. (14a) given as

$$B = A - C - K,$$

where

$$B = U_R \cdot \frac{\partial U_R}{\partial R} + \frac{U_\phi}{R} \cdot \frac{\partial U_R}{\partial \phi} - \frac{{U_\phi}^2}{R},$$

$$A = Gr \cos \Delta,$$

$$C = \left[\frac{\partial P}{\partial R} - \frac{\partial^2 U_R}{\partial R^2} - \frac{1}{R^2} \cdot \frac{\partial^2 U_R}{\partial \phi^2} - \frac{1}{R} \cdot \frac{\partial U_R}{\partial R} \right],$$

$$K = \left[\frac{2}{R^2} \cdot \frac{\partial V}{\partial \phi} + \frac{U_R}{R^2} + \frac{U_R}{Da} + Ha^2 \right],$$

$$U_R = U_{Ri,j}\ , \tag{18b}$$

$$U_\emptyset = U_{\emptyset i,j}, \tag{18c}$$

$$\frac{\partial U_R}{\partial R} = \frac{U_{Ri+1,j} - U_{Ri,j}}{\Delta R}\ , \tag{18d}$$

$$\frac{U_\emptyset}{R} = \frac{U_{\emptyset i,j}}{R_{i,j}}, \tag{18e}$$

$$\frac{\partial U_R}{\partial \emptyset} = \frac{U_{Ri,j+1} - U_{Ri,j}}{\Delta \emptyset}, \tag{18f}$$

$$\frac{\partial^2 U_R}{\partial R^2} = \frac{U_{Ri+1,j} - 2U_{Ri,j} + U_{Ri-1,j}}{\Delta R^2}, \tag{18g}$$

$$\frac{\partial P}{\partial R} = \frac{\Delta P}{\Delta R}, \tag{18h}$$

$$\frac{\partial^2 U_R}{\partial \emptyset^2} = \frac{U_{Ri,j+1} - 2U_{Ri,j} + U_{Ri,j-1}}{\Delta \emptyset^2}, \tag{18i}$$

$$\frac{{U_\emptyset}^2}{R} = \frac{\left(U_{\emptyset i,j}\right)^2}{\Delta R}\ , \tag{18j}$$

$$\frac{1}{R^2} = \frac{1}{{R^2}_{i,j}}, \tag{18k}$$

$$\frac{U_R}{R^2} = \frac{U_{Ri,j}}{{R^2}_{i,j}}, \tag{18l}$$

$$\frac{\partial U_\emptyset}{\partial \emptyset} = \frac{U_{\emptyset i,j+1} - U_{\emptyset i,j}}{\Delta \emptyset}, \tag{18m}$$

$$\frac{2}{R^2} = \frac{2}{R^2{}_{i,j}}, \tag{18n}$$

$$\frac{U_R}{Da} = \frac{U_{Ri,j}}{Da}, \tag{18o}$$

Substituting Eqs. (18b) to (18o) into Eq. (14a) yields

$$i, j = \left(\frac{\begin{array}{c} Gr\cos\theta - \frac{1}{\Delta R}\left(\frac{U_{\emptyset i+1,j}}{R_{i,j}} - \Delta P\right) + \frac{U_{Ri+1,j} - U_{Ri-1,j}}{\Delta R} \\ + \frac{1}{R^2_{i,j}\Delta\emptyset}\left(\frac{U_{i,j+1} + U_{i,j-1}}{\Delta\emptyset} - 2\left(U_{\emptyset i,j+1} - U_{\emptyset i,j}\right)\right) \\ - \frac{1}{R_{i,j}}\left(\frac{U_{\emptyset i,j} \cdot U_{Ri,j+1}}{\Delta\emptyset} + \left(U_{\emptyset i,j}\right)^2\right) - Ha^2 \end{array}}{\frac{1}{\Delta R}\left(\left(U_{Ri+1,j} - U_{Ri,j}\right) + \frac{2}{\Delta R}\right) + \frac{1}{R_{i,j}}\left(\frac{1}{\Delta R} - \frac{U_{\emptyset i,j}}{\Delta\emptyset}\right) + \frac{1}{R^2_{i,j}}\left(\frac{2}{\Delta\emptyset^2} + 1\right) + \frac{1}{Da}} \right), \tag{18p}$$

$$U_{R_{i,j}} = \left(\frac{\begin{array}{c} Gr\cos\theta - C\left(\frac{U_{Ri+1,j}}{R_{i,j}} - \Delta P\right) + \frac{U_{Ri+1,j} - U_{Ri-1,j}}{\Delta R} \\ + D_{i,j}\left(\frac{U_{Ri,j+1} + U_{Ri,j-1}}{\Delta\emptyset} - 2\left(U_{\emptyset i,j+1} - U_{\emptyset i,j}\right)\right) \\ - A_{i,j}\left(\frac{U_{\emptyset i,j} \cdot U_{\emptyset i,j+1}}{\Delta\emptyset} + \left(U_{\emptyset i,j}\right)^2\right) - Ha^2 \end{array}}{C\left(\left(U_{Ri+1,j} - U_{Ri,j}\right) + \frac{2}{\Delta R}\right) + A_{i,j}\left(C - \frac{U_{\emptyset i,j}}{\Delta\emptyset}\right) + B_{i,j}\left(\frac{2}{\Delta\emptyset^2} + 1\right) + \frac{1}{Da}} \right), \tag{18q}$$

where

$$A_{i,j} = \frac{1}{R_{i,j}}, \tag{18r}$$

$$B_{i,j} = \frac{1}{R^2_{i,j}}, \tag{18s}$$

$$C = \frac{1}{\Delta R}. \tag{18t}$$

2.5.3. Azimuthal direction (Ø)

The mathematical expression below explains the FDA of normalized momentum governing equation in an azimuthal direction from Eq. (15a) given as

$$B = A - L + D,$$

where

$$B = \left[U_R \cdot \frac{\partial U_\emptyset}{\partial R} + \frac{U_\phi}{R} \cdot \frac{\partial U_\emptyset}{\partial \phi} + \frac{U_R U_\emptyset}{R}\right],$$

$$A = Gr \ \sin\theta,$$

$$L = \left[\frac{1}{R} \cdot \frac{\partial p}{\partial \phi} - \frac{\partial^2 U_\emptyset}{\partial R^2} - \frac{1}{R^2} \cdot \frac{\partial^2 U_\emptyset}{\partial \phi^2}\right],$$

$$D = \left[\frac{\partial U_R}{\partial R} + \frac{2}{R^2} \cdot \frac{\partial U_R}{\partial \phi} - \frac{U_\phi}{R^2} - \frac{U_\phi}{Da}\right],$$

$$\frac{U_R \partial U_\emptyset}{\partial R} = \frac{U_{Ri,j} \cdot \left(U_{\emptyset i+1,j} - U_{\emptyset i,j}\right)}{\Delta R}, \tag{19a}$$

$$\frac{U_\emptyset}{R} \cdot \frac{\partial U_\emptyset}{\partial \emptyset} = \frac{U_{\emptyset i,j}}{R_{i,j}} \cdot \frac{\left(U_{\emptyset,i,j+1} - U_{\emptyset i,j}\right)}{\Delta \emptyset}, \tag{19b}$$

$$\frac{U_R U_\emptyset}{R} = \frac{U_{Ri,j} \cdot U_{\emptyset i,j}}{R_{i,j}}, \tag{19c}$$

$$\frac{1}{R} \cdot \frac{\partial P}{\partial \emptyset} = \frac{\cdot P}{R_{i,j} \Delta \emptyset}, \tag{19d}$$

$$\frac{\partial^2 U_\emptyset}{\partial R^2} = \frac{U_{\emptyset i+1,j} - 2U_{\emptyset i,j} + U_{\emptyset i-1,j}}{\Delta R^2}, \tag{19e}$$

$$\frac{1}{R^2} \cdot \frac{\partial^2 U_\emptyset}{\partial \emptyset^2} = \frac{U_{\emptyset i,j+1} - 2U_{\emptyset i,j} + U_{\emptyset i,j-1}}{R^2_{i,j} \ \Delta \emptyset^2}, \tag{19f}$$

$$\frac{2}{R^2} \cdot \frac{\partial U_R}{\partial \emptyset} = \frac{2}{R^2_{i,j}} \frac{\left(U_{Ri,j+1} - U_{Ri,j}\right)}{\Delta \emptyset}, \tag{19g}$$

$$\frac{U_\emptyset}{R^2} = \frac{U_{\emptyset i,j}}{R^2{}_{i,j}}, \tag{19h}$$

$$\frac{U_\emptyset}{Da} = \frac{U_{Ri,j}}{Da}. \tag{19i}$$

Substituting Eqs. (19a) to (19i) into Eq. (15a) gives

$$K\,(A + B + C) = D - E - M\,(F + G + H) + N\,(I + J)\,, \tag{19.1a}$$

where

$$K = U_{\emptyset i,j}, \tag{19.1b}$$

$$A = \left(\frac{1}{\Delta R}\left(\frac{2}{\Delta R} - U_{Ri,j}\right)\right), \tag{19.1c}$$

$$B = \frac{1}{R_{i,j}}\left(\left(\frac{U_{\emptyset i,j+1} - U_{\emptyset i,j}}{\Delta \emptyset}\right) + U_{Ri,j}\right), \tag{19.1d}$$

$$C = \frac{1}{R_{i,j}^2}\left(\frac{2}{\Delta \emptyset^2} + 1\right) + \frac{1}{Da}, \tag{19.1e}$$

$$D = Gr \sin\theta, \tag{19.1f}$$

$$E = \frac{\theta P}{R_{i,j}\ \theta \emptyset}, \tag{19.1g}$$

$$M = \frac{1}{\Delta R}, \tag{19.1h}$$

$$F = \left(U_{Ri,j} \cdot U_{\emptyset i+1,j}\right), \tag{19.1i}$$

$$G = \left(U_{Ri+1,j} - U_{Ri,j}\right), \tag{19.1j}$$

$$H = \left(\frac{U_{\emptyset i+1,j} + U_{\emptyset i-1,j}}{\Delta R}\right), \tag{19.1k}$$

$$N = \frac{1}{R_{i,j}^2\ \Delta \emptyset}, \tag{19.1l}$$

$$I = \left(\frac{U_{\emptyset i,j+1} + U_{\emptyset i,j-1}}{\Delta \emptyset}\right), \tag{19.1m}$$

$$J = 2\left(U_{Ri,j+1} - U_{Ri,j}\right). \tag{19.1n}$$

Further simplification gives

$$U_{\emptyset i,j} = \left(\frac{\begin{array}{c} Gr \sin\theta - \frac{\Delta P}{E_{i,j}} - C\left(\left(U_{Ri,j} \cdot U_{\emptyset i+1,j}\right) + \left(U_{Ri+1,j} - U_{Ri,j}\right) + \frac{U_{\emptyset i+1,j} + U_{\emptyset i-1,j}}{\Delta R}\right) \\ + B_{i,j}\left(\left(\frac{U_{\emptyset i,j+1} + U_{\emptyset i,j-1}}{\Delta \emptyset}\right) + 2\left(U_{Ri,j+1} - U_{Ri,j}\right)\right) \end{array}}{\left(C\left(\frac{2}{\Delta R} - U_{Ri,j}\right)\right) + D_{i,j}\left(\left(\frac{U_{\emptyset i,j+1} - U_{\emptyset i,j}}{\Delta \emptyset}\right) + U_{Ri,j}\right) + A_{i,j}\left(\frac{2}{\Delta \emptyset^2} + 1\right) + \frac{1}{Da}}\right), \tag{19.2a}$$

where

$$A_{i,j} = \frac{1}{R_{i,j}^2}, \tag{19.2b}$$

$$B_{i,j} = \frac{1}{R_{i,j}^2\ \Delta\emptyset}, \tag{19.2c}$$

$$C = \frac{1}{\Delta R\ \ Re}, \tag{19.2d}$$

$$D_{i,j} = \frac{1}{R_{i,j}}, \tag{19.2e}$$

$$E_{i,j} = \frac{1}{R_{i,j}\ \Delta\emptyset}. \tag{19.2f}$$

2.5.4 Energy Transport Equation

The mathematical expression below shows the finite difference analogue for the normalized energy transport governing equation from Eq. (16) given as

$$\frac{\partial^2 T}{\partial R^2} + \frac{1}{R^2} \cdot \frac{\partial^2 T}{\partial \emptyset^2} + \frac{1}{R} \cdot \frac{\partial T}{\partial R} = Pr \left[U_R \cdot \frac{\partial T}{\partial R} + U_\emptyset \cdot \frac{\partial T}{R \partial \emptyset} \right]$$

$$\frac{\partial T}{\partial R} = \frac{-T_{i,j}}{\Delta R} \tag{20a}$$

$$\frac{\partial^2 T}{\partial R^2} = \frac{T_{i+1,j} - 2T_{i,j} + T_{i-1,j}}{\Delta R^2} \tag{20b}$$

$$\frac{\partial T}{R \partial \emptyset} = \frac{T_{i,j+1} - T_{i,j}}{R \Delta \emptyset} \tag{20c}$$

$$\frac{\partial^2 T}{\partial \emptyset^2} = \frac{T_{i,j+1} - 2T_{i,j} + T_{i,j-1}}{\Delta \emptyset^2} \tag{20d}$$

Substituting equations (20a – 20d) into equation 16, yields

$$\mathrm{L} + \mathrm{I} + \mathrm{S} = \mathrm{T}\,(\mathrm{E} + \mathrm{N}) \tag{20.1a}$$

Where

$$\mathrm{L} = \frac{T_{i+1,j} - 2T_{i,j} + T_{i-1,j}}{\Delta R^2} \tag{20.1b}$$

$$\mathrm{I} = \frac{1}{R_{i,j}^2} \cdot \frac{\left(T_{i,j+1} - 2T_{i,j} + T_{i,j-1}\right)}{\Delta \emptyset^2} \tag{20.1c}$$

$$\mathrm{S} = \frac{1}{R_{i,j}} \cdot \frac{\left(T_{i+1,j} - T_{i,j}\right)}{\Delta R} \tag{20.1d}$$

$$\mathrm{T} = Pr \tag{20.1e}$$

$$\mathrm{E} = U_{Ri,j}\frac{\left(T_{i+1,j} - T_{i,j}\right)}{\Delta R} \tag{20.1f}$$

$$\mathrm{N} = U_{\emptyset i,j}\frac{\left(T_{i,j+1} - T_{i,j}\right)}{R_{i,j}\Delta\emptyset} \tag{20.1g}$$

$$\mathrm{P(R)} = \mathrm{Y} + \mathrm{D} - \mathrm{U} - \mathrm{C} - \mathrm{T} \tag{20.2a}$$

Where

$$\mathrm{P} = T_{i,j} \tag{20.2b}$$

$$\mathrm{R} = \left(\frac{-2}{\Delta R^2} - \frac{2}{R_{i,j}^2\Delta\emptyset^2} - \frac{1}{R_{i,j}\Delta R} + \frac{Pr\cdot U_{R_{i,j}}}{\Delta R} + \frac{Pr\cdot U_{\emptyset_{i,j}}}{R_{i,j}\Delta\emptyset}\right) \tag{20.2c}$$

$$\mathrm{Y} = \frac{Pr\left(U_{Ri,j}\cdot T_{i+1,j}\right)}{\Delta R} \tag{20.2d}$$

$$\mathrm{D} = \frac{Pr\cdot\left(U_{\emptyset i,j}\cdot T_{i,j+1}\right)}{R_{i,j}\Delta\emptyset} \tag{20.2e}$$

$$\mathrm{U} = \left(\frac{T_{i+1,j} + T_{i-1,j}}{\Delta R^2}\right) \tag{20.2f}$$

$$\mathrm{C} = \left(\frac{T_{i,j+1} + T_{i,j-1}}{R_{i,j}^2\Delta\emptyset^2}\right) \tag{20.2g}$$

$$\mathrm{T} = \frac{\left(T_{i+1,j}\right)}{R_{i,j}\Delta R} \tag{20.2h}$$

$$T_{i,j} = \left[\frac{C\frac{\left(U_{Ri,j}\cdot T_{i+1,j}\right)}{\Delta R} + \frac{U_{\emptyset i,j}\left(T_{i,j+1}\right)}{R_{i,j}\Delta\emptyset} - \left(\frac{T_{i+1,j}+T_{i-1,j}}{\Delta R^2}\right) - \left(\frac{T_{i,j+1}+T_{i,j-1}}{R_{i,j}^2\Delta\emptyset^2}\right) - \frac{T_{i+1,j}}{R_{i,j}\Delta R} +}{\frac{-2}{\Delta R^2} - \frac{2}{R_{i,j}^2\Delta\emptyset^2} - A_{i,j} + C\left(\frac{U_{Ri,j}}{\Delta R} + \frac{U_{\emptyset i,j}}{R_{i,j}\Delta\emptyset}\right)}\right] \tag{20.3a}$$

Where

$$C = Pr, \tag{20.3b}$$

$$A_{i,j} = \frac{1}{R_{i,j}\Delta R} \tag{20.3c}$$

3. The Method of Solution

3.1. Solution techniques

The dimensionless governing equation with its associated boundary conditions were solved numerically using finite difference method adopting Gauss–Seidel technique. For the discretization

of the governing equations, the central difference quotients were used for the second-order derivatives and forward difference were used for the first-order derivative. The algebraic equations obtained for each variable were solved by simple form of Gauss–Seidel iterative procedure because it generates a well-refined estimate of the solution and its error could be controlled by the number of iterations. The central difference quotients were used to appropriate the derivatives in both radial (R) and Azimuthal (Ø) directions.

Convergence criteria (10^{-6}) is chosen for all dependent variables and the value of (0.1) is used for the under relaxation parameters the approach similar to [2]. The number of grid points is taken as (48×192) with uniform spaced mesh in both R and Ø directions. Consequently, the Nusselt numbers, surface heat transfer coefficient, velocity, and temperature distributions were obtained from the numerical simulation once the convergence criteria was satisfied.

3.2. Computational procedure

The whole cross-section for laminar natural convection flow in an elliptic enclosure filled with porous medium was used in the numerical computation. The velocity fields were numerically evaluated from the momentum transport equations and its associated boundary conditions. The velocity obtained was then used for the evaluation of energy transport equations for the generation of temperature distribution for the fluid region.

Computed values for Nusselt number, average or mean velocity, flow temperature distributions, effect of eccentricity on the tube, and heat transfer rate in the enclosure were evaluated by varying the following dimensionless controlling parameters: Grashof number, Darcy number, Hartmann number, and enclosure inclination angle.

3.3. Heat transfer analysis

After obtaining the stream function and temperature distribution, the flow and heat transfer characteristics are easily determined. The heat transfer rate are presented in terms of local and average Nusselt numbers, that is, Nu and Nu_a [16].

Nusselt number is a nondimensional parameter indicative of the ratio of energy convection to conduction [31]:

$$Nu = \frac{hD_h}{k}. \tag{21a}$$

For equation of conduction

$$q_{con} = k\frac{dT}{dr} \quad . \tag{21b}$$

Similarly for convection heat transfer mechanism,

$$q_{conv.} = h(T_w - T_f). \tag{21c}$$

If assumes that the heat conduction equal to heat convection, that is,

$$q_{con} = q_{conv} \tag{21d}$$

implies that,

$$k\frac{dT}{dr} = h(T_w - T_f). \tag{21e}$$

Making h the subject of the equation gives,

$$h = \frac{K\frac{dT}{dr}}{T_w - T_f}. \tag{21f}$$

From Eq. (21a), that is, Nu $= \frac{hD_h}{k}$, Nu becomes,

$$Nu = \frac{hD_h}{k} = \frac{k\frac{dT}{dr}}{\left(T_w - T_f\right)\mathrm{k}}.D_h \tag{21g}$$

$$Nu = \frac{\frac{dT}{dr}}{\left(T_{w-}T_f\right)} \times D_h, \tag{21h}$$

where

$$D_h = \frac{4A}{P}, \tag{21i}$$

$$A = \text{cross} - \text{sectional area} \tag{21j}$$

$$P = \text{watted perimeter}, \tag{21k}$$

$$D_h = \frac{4\pi\,(ab)}{\pi\,(a+b)} = \frac{4ab}{a+b} = \frac{4a\sqrt{1-e^2}}{1+\sqrt{1-e^2}}. \tag{21l}$$

4. Grid Testing and Validation of the Numerical Results

To verify the grid independence of the solution scheme, numerical experiments were performed as shown in Table 1. Different mesh sizes were used for the case of resolution at Gr $= 10^6$, Ha = 25, Da $= 10^{-3}$, $\theta = 30^0$, $e = 0.8$, and Pr = 0.7.

Table 1. Comparison of average Nusselt number along the bottom heated wall of the elliptic enclosure for different grid resolution at Gr $= 10^6$, Ha = 25, Da $= 10^{-3}$, $\boldsymbol{\theta} = 30^0$, $\boldsymbol{e} = 0.8$, Pr = 0.7

Mesh sizes in radial and azimuthal directions	18×66	33×129	48×192	63×255
NU_a	3.33917	3.34816	3.35077	3.35867

The present code is tested for grid independence by calculating the average Nusselt number at the bottom heated wall of the enclosure. Convergence criteria (10^{-6}) is chosen for all dependable variables and the value of (0.1) is used for the relaxation parameters the approach similar to Ref. [2]. It is found that a grid size (48 × 192) ensured a grid independent solution for the present study as shown in Table 1.

The results of the present work for $0 \leq e \leq 1$ was compared with the one reported by Bello–Ochende and Adegun [18] on perturbation analysis of combined natural and forced convection in a tilted elliptic cylinder. The comparison was made for the above parametric range, the results showed that for $e = 0.866$, the local Nusselt number exhibited significant dependence on the azimuthal angle and also indicated that the optimal value of mean Nusselt number (Nu_a) occurred at $e = 0.866$. When compared with the present study, there was an excellent agreement. Also, the work reported by Adegun and Oladosu [19] on scale analysis of natural and forced convective heat transfer in an elliptic conduit for the parametric range $0 \leq e \leq 1$, the results showed that the generalized Nusselt number is dependent solely on the eccentricity of the ellipse and that the average Nusselt number at the end of minor axis is greater than that of major axis, there is an excellent agreement when compared with the present work. When the developed algorithm is simulated for, e value = 0.866, the highest rate of heat transfer is noticed at the end of minor axis of the configuration as reported and predicted by Bello-Ochende, Adegun [18], and Abdel-Wahed and colleagues [15], there is in excellent agreement when compared.

In order to further establish the accuracy of the mathematical model and the correctness of the numerical solution, the present numerical results were further compared with the most relevant results in the literature. The average Nusselt number at the heated bottom wall had been compared with the corresponding results reported by Mahfouz, 2011 related with the buoyancy driven flow in an inclined elliptic enclosure as shown in Table 2. The comparison was made using the inner wall which is relevant to the present work in his results and the following dimensionless parameters were considered: Pr = 0.7, Ra $= 10^5$, $\theta = 90^0$, Ha = 0. Enclosure geometry (in terms of aspect ratio) compared with the corresponding values of eccentricity and the controlling parameters in the present work shows good agreement

Further comparison was also performed on the numerical computation of magneto-thermal convection of water in a vertical cylindrical enclosure reported by Masato. The comparison was made on the average Nusselt number at the hot plate for the circular electric coil with 2.5 or 5 times the diameter of the cylindrical enclosure in a gravitational field (the system with magnetic field). The following dimensionless parameters were compared: Ra= 10^4, Ha $\neq$0, Pr = 5.85. When the present numerical algorithm is simulated using Pr = 5.85, Ra $= 10^4$, Ha $\neq$ 0, the average Nusselt numbers when compared showed a very good agreement as shown in Table 2

In the same vein, the results obtained were compared with the work reported by Ghasemi and colleagues,2012, the results obtained on the average Nusselt number for the following dimensionless parameters:$e = 0.9$, major axis ratio (0.6), inclination angle (90^0), Ra $= 10^5$, Ha $= \Delta = 0$ gives a good agreement when compared with the present work.

Also, the results obtained in this work were compared with the results reported by Sakalis and colleagues. 2002, with thermally developing flow in elliptic ducts. The comparison is made using a

Table 2. Comparison of average Nusselt number (NU_a)

S/No	Present work	Published results	Deviation %
1	Ra = $1.86x \times 10^4$, Pr = 0.7, Ha = $\Delta = 0$, $\theta = 90^0$, $e = 0.9$	Mahfouz (2011) Inner wall, Ra = 1.86 x 10^4, Pr = 0.7, Ha = $\Delta = 0$, $\theta = 90^0$, $e = 0.9$(inclined elliptic enclosure)	
	$NU_a = 3.35341$	$NU_a = 3.179$	5.49%
2	Ra $= 10^4$, Pr = 5.85 , Ha $\neq 0$	Masato (2005) (the system with magnet) Ra = 10^4, Pr = 5.85, Ha $\neq$0 (circular and cylindrical enclosures)	
	$NU_a = 3.33074$	$NU_a = 3.3856$	1.62%
3	Ra = $10^4 - 10^6$, $e = 0.9$, ; Ha = $\Delta = 0$, $\theta = 30^0$, Pr = 0.7, Aspect ratio = 0.6	Ghasemi and colleagues (2012) Ra = 10^4–10^5, e = 0.9, Pr = 0.7, aspect ratio = 0.6, , $\theta = 30^0$ (circular enclosure)	
	$NU_a = 3.35241$	$NU_a = 2.9978$	11.82%
4	Ra = $10^4 - 10^6$, $e = 0.8$, $NU_a = 3.35241$	Hajjat and colleagues (2013) Ra = $10^4 - 10^6$, e = 0.8 $NU_a = 3.321852$ (circular and elliptic enclosures)	0.92%
5	Aspect ratio = 0.8, Tw = constant.	Sakalis and colleagues (2002) Aspect ratio, 0.8, Tw = constant (ellipticduct)	
	$NU_a = 3.35377$	$NU_a = 3.672$	8.66%

different aspect ratio, (0.6), Tw = constant, that is, constant wall temperature with the present work for different corresponding eccentricity, a good agreement is obtained when the average number is compared as shown in the Table 2. The study of computational fluid dynamics (CFD) analysis of laminar natural convection in a circular cylinder to its elliptic enclosure reported by Hojjat and colleagues. 2013 was also compared with this current study for Ra $= 10^4$ to 10^6, different aspect ratio (0.6), the average Nusselt number shows good agreement.

5. Results and Discussion

Having studied and validated the numerical method employed in the present work, the effects of salient geometric parameters (eccentricity, e, and enclosure inclination angles) and fluid properties (Hartmann, Darcy, and Grashof numbers) on the rate of heat transfer in a steady-state 2D laminar MHD natural convection flow in an inclined elliptic enclosure filled with fluid saturated porous medium has been investigated and discussed.

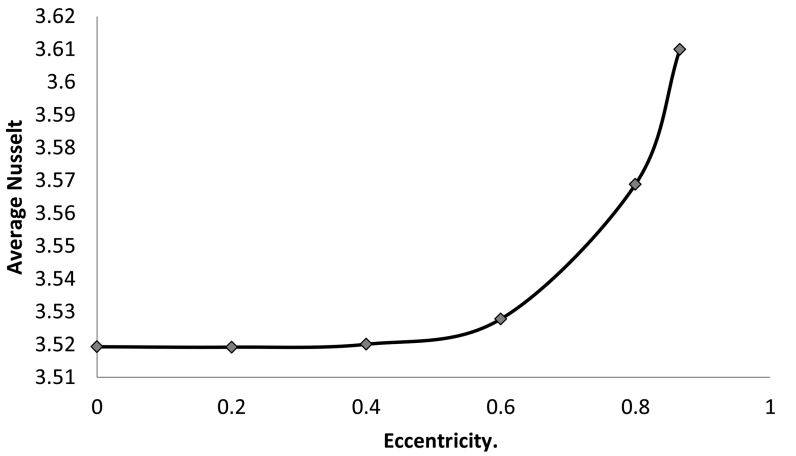

Fig. 2. Effects of different values of eccentricity, e, on the average Nusselt number. [Color figure can be viewed in the online issue, which is available at wileyonlinelibrary.com/journal/htj.]

5.1. Effect of eccentricity on local and average Nusselt numbers

Figure 4 shows e values considered in the study. The variation of the local Nusselt number with respect to azimuthal angle at the bottom heated wall of the elliptic configuration along the minor and major axes are presented. For $e = 0$, the distribution pattern is almost symmetrical about the point located at $\Phi = 180^0$ angular position. The optimum heat transfer of Nu = 3.36 is at $\Phi = 120^0$ while the minimum of Nu = 3.24 is at $\Phi = 180^0$. The distribution pattern of $e = 0.2$ is almost similar to that of $e = 0$ in its behavior except for the rate of heat transfer that is higher about the point located at $\Phi = 180^0$ angular position. In a nutshell, in the parametric range $0 \leq e \leq 0.2$, the difference between the heat transfer rate at the end of major and minor axes is insignificant.

Above $e = 0.2$, more heat is transferred from the end of minor axis of the enclosure, that is, Nusselt numbers at the end of minor axis are greater than the major axis (minor axis = 4.2 and major axis = 3.0) of the elliptic enclosure. It is also observed from the plot that the higher the value of eccentricity, e, the higher the rate of heat transfer between the parametric range considered, that is, $0.4 \leq e \leq 0.8$ but decreases within the parametric range $180^0 \leq \Phi \leq 270^0$. Again, a critical eccentricity, $e = 0.8$ is attained for optimum heat transfer by convection at the end of the minor axis. When the developed algorithm is simulated for, e value = 0.866, as shown in Fig. 3, the highest rate of heat transfer is noticed at the end of the minor axis of the configuration as reported and predicted by Bello-Ochende and Adegun [18], and Abdel-Wahed and colleagues [15]. In the same vein, it is observed that the rate of heat transfer at $\Phi = 135^0$ and 235^0, respectively, is almost the same for all eccentricities considered.

Figure 5 illustrates the variation of average Nusselt number with various values of eccentricity of the ellipse at the end of the minor axis. It is observed in the figure that average Nusselt number increases monotonically for the parameter range $0 \leq e \leq 0.6$, the difference between the heat transfer rate along the minor axis is not significant. Above e = 0.6, it is noticed that the higher the value of eccentricity, e, the higher the rate of heat transfer. Also, between the parametric range $0.6 \leq e < 1$,

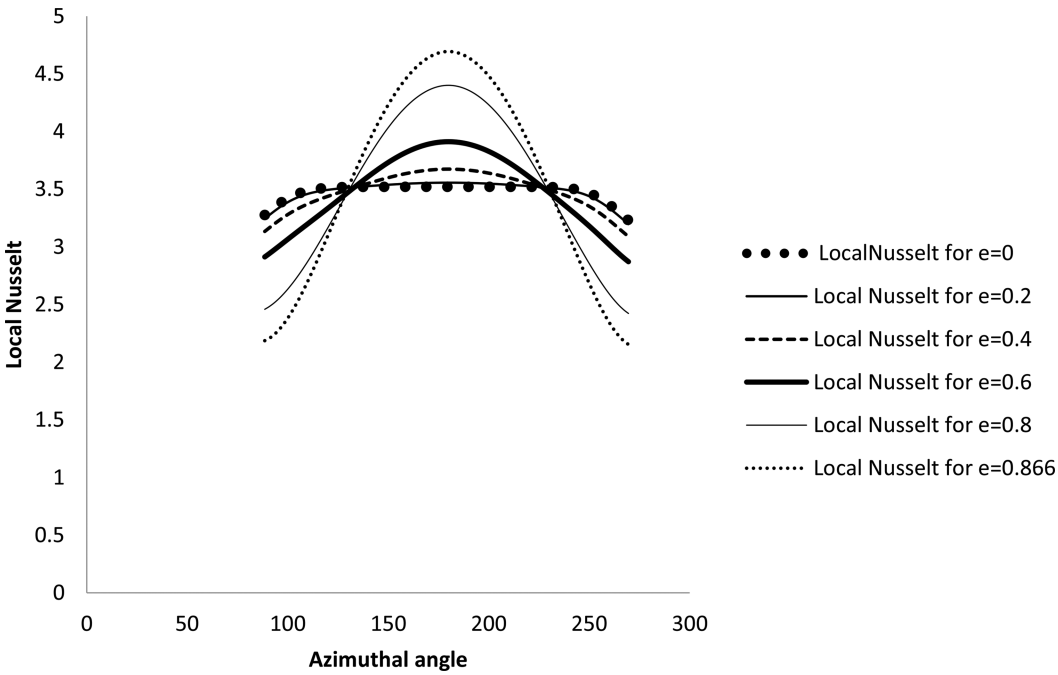

Fig. 3. Effects of local Nusselt number on azimuthal angle for different eccentricity.

heat transfer is no longer by convection only, conduction also occurred, a reason for the sudden rise in the rate of heat transfer.

A critical eccentricity, $e = 0.8$, is attained for optimum heat transfer, therefore 0.8 is the critical value for highest heat transfer by convection which compares well with published journals.

5.2. Effect of enclosure inclination angle on average Nusselt number

Figure 6 depicts the relationship between the average Nusselt number and angle of inclination. The plot explains a monotonical increment between the parametric rang $0^0 \leq \theta \leq 58^0$, the inclination is not significant within this range. Above58^0, as is evidently observed from the figure, inclination increases considerably with the rate of heat transfer for the parametric range $58^0 \leq \theta \leq 90^0$

5.3. Effect of Hartmann number

Figure 7 presents the variation of velocity distribution in a radial direction along the minor axis of the enclosure for various Hartmann numbers (Ha = 0, 2 5, 50), for an inclination angle of $\theta = 30^o$, at Gr = 10^6, Da = 10^{-3}, Pr = 0.7

The Hartmann number is an indication of existence of MHD flow. It can be observed from the figure that when there is magnetic field influence (Ha = 25, 50) and when the magnetic influence is negligible (Ha = 0) on the field flow and thermal characteristics in the enclosure.

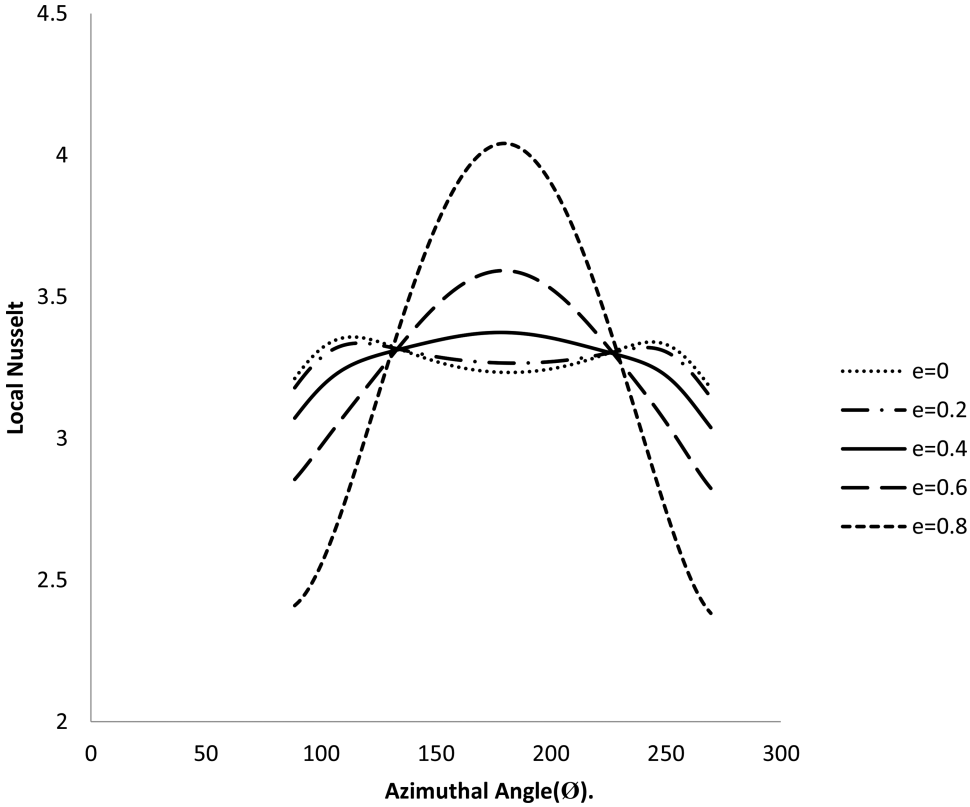

Fig. 4. Effects of different values of eccentricity on local Nusselt number at the bottom wall for various Azimuthal angles (J1) along the major axis of the enclosure.

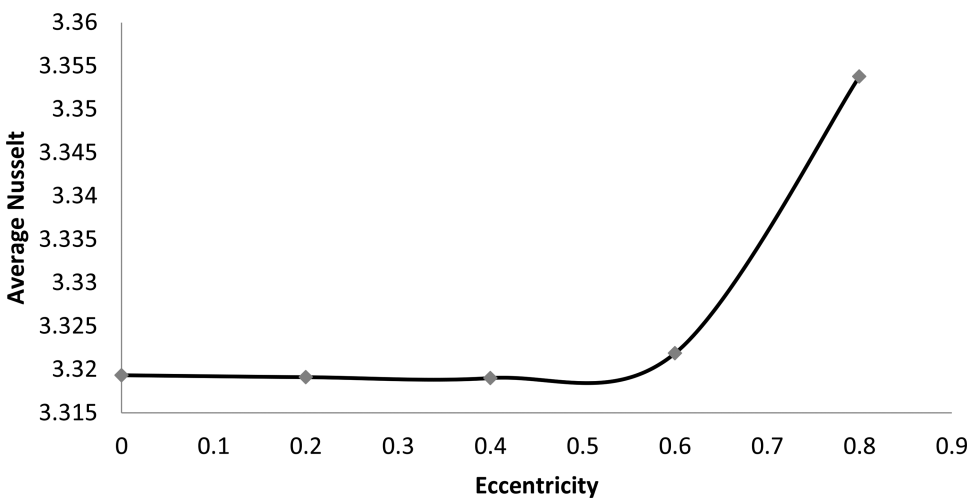

Fig. 5. Effect of eccentricity on the average Nusselt number. [Color figure can be viewed in the online issue, which is available at wileyonlinelibrary.com/journal/htj.]

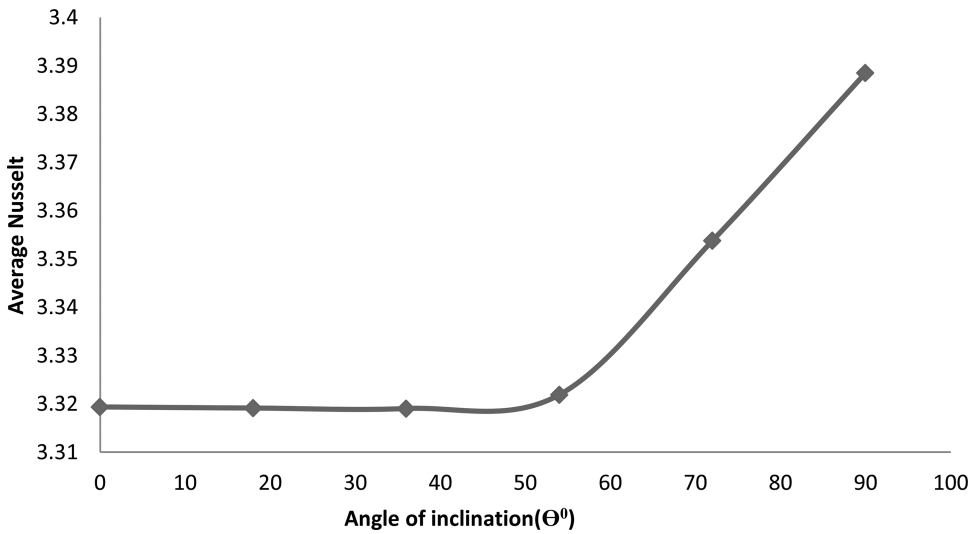

Fig. 6. Effect of enclosure inclination angle on the average Nusselt number. [Color figure can be viewed in the online issue, which is available at wileyonlinelibrary.com/journal/htj.]

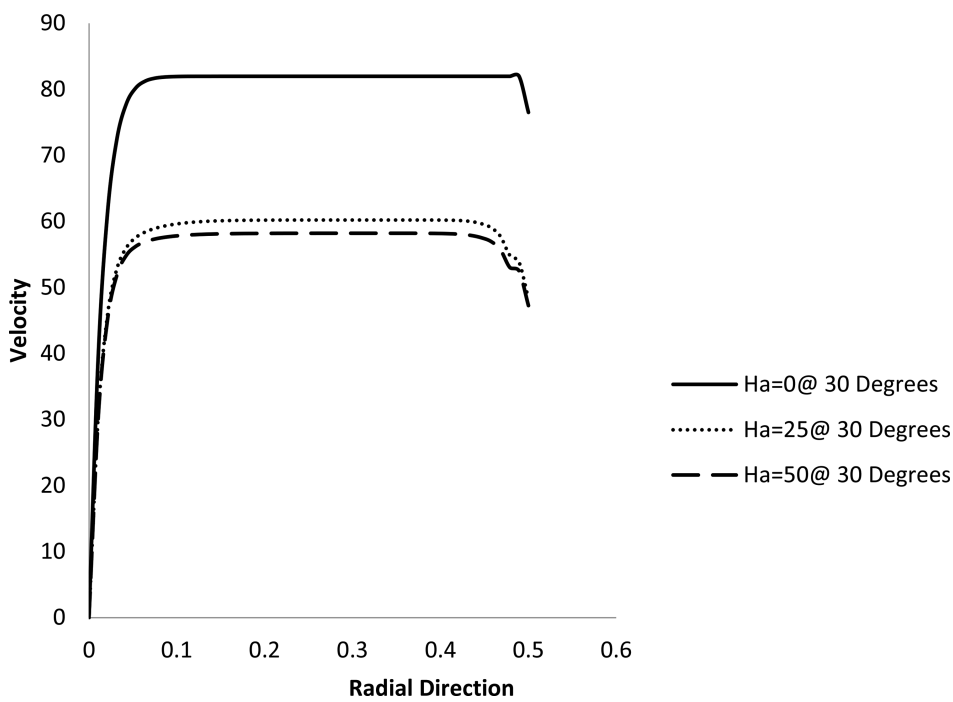

Fig. 7. Velocity distribution in radial direction of the enclosure for different values of Hartmann numbers.

When the Hartmann number is zero (Ha = 0), the flow circulation (dimensionless velocity distribution) becomes stronger, because of buoyancy force due to the natural convection effect, which is the dominant force in the enclosure, that is, heat is transferred by convection. It can be seen from the figure that at Ha = 0, the flow circulation is very strong as a result of no magnetic field effect.

Contrary is the case when Hartmann number increases (Ha = 25, 50), the Lorentz or Laplace force, a force on the point charge due to electromagnetic force. This force created as a result of magnetic field influence becomes greater than the buoyancy force due to natural convection which causes a reduction in field flow circulation since Lorentz force suppresses the convection current and consequently leads to a reduction in velocity distribution.

Also, it is observed in the figure that the flow circulation becomes weak at the core along the minor axis of the enclosure due to strong mixing of the fluid, that is, the presence of cold and hot fluid results in flow circulation reduction at the core

5.4. Effect of Darcy number

Figure 8 explains the variation of dimensionless velocity distribution in radial direction along the minor axis of the enclosure for various values of Darcy numbers (Da = 10^{-3}, 10^{-4}, 10^{-5}), Ha = 25, Gr = 10^6, $\theta = 30^o$, Pr = 0.7

When Darcy is high (Da = 10^{-4}) considering the positive side of the plot, a strong intensity of fluid circulation can be observed inside the elliptic enclosure. The flow circulations are higher at the enclosure heated bottom wall and weak at the cold top side wall of the enclosure due to a no-slip boundary condition. As can be seen in the figure, as the Darcy number decreases from Da = 10^{-4} to 10^{-5}, the flow circulation becomes weak. Mixture of cold and hot fluid at the core of the enclosure causes reduction in the flow circulation (velocity distribution) along the radial direction of the enclosure. When Darcy is at10^{-3}, it behaves in a similar manner to that of 10^{-4} but in an opposite direction. Also, it is observed from the figure that it increases at the core of the enclosure while Darcy at 10^{-4} starts decreasing and this compares well with the work reported by Ahmed and colleagues, 2012, that used the same range of values but in a trapezoidal enclosure

5.5. Effect of Grashof number

Figure 9 illustrates the dimensionless velocity distribution in the radial direction (RR) along the minor axis of the enclosure for various Grashof numbers (Gr = 10^4, 10^5, 10^6), Ha = 25, Da = 10^{-3}, $\theta = 30^o$, Pr = 0.7

When the value of Grashof number is 10^4, the magnitude of fluid flow circulation is small due to the slight effect of convection when Grashof number is low; but as the value of Grashof number increases from Gr = 10^5 to 10^6 because of buoyancy force as a result of the natural convection effect, the field flow circulation (in terms of velocity distribution) in the enclosure strongly increases.

At the core of the enclosure, there is reduction in flow circulation due to strong mixing of cold and hot fluid.

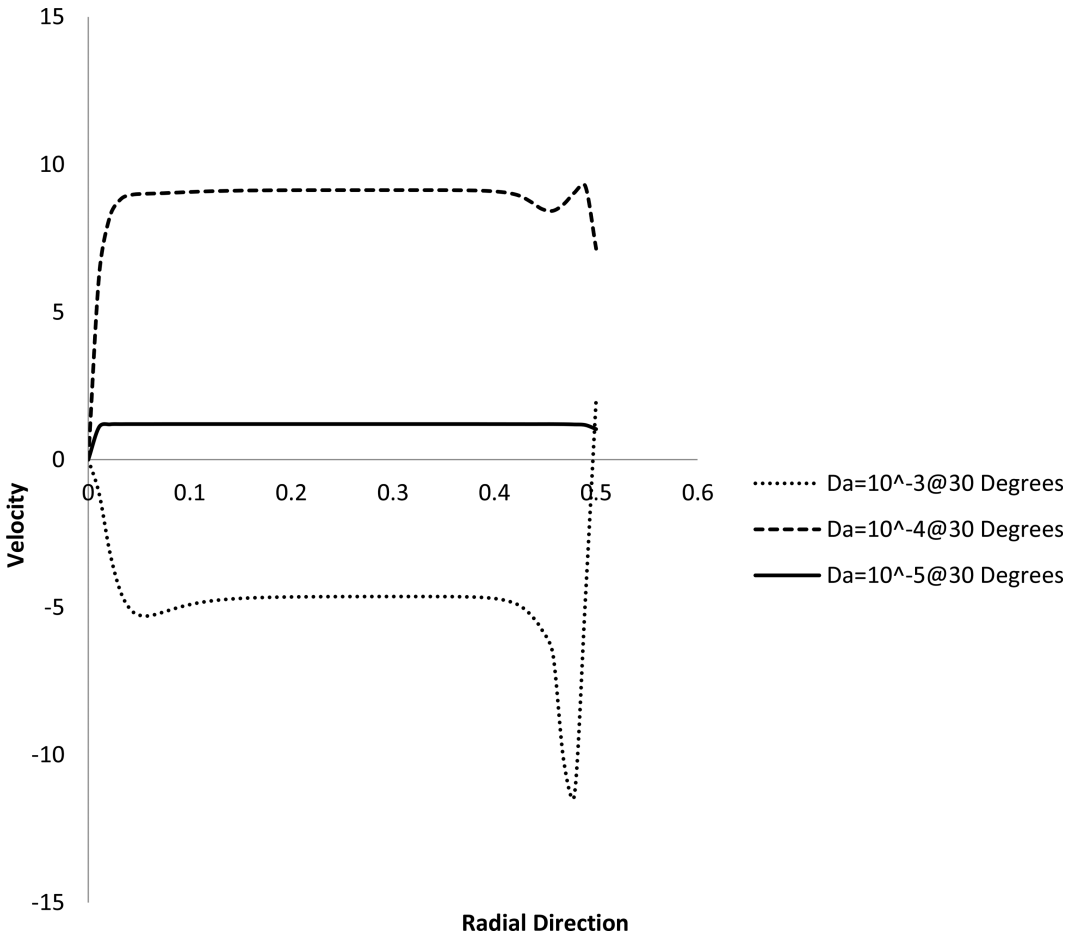

Fig. 8. Velocity distribution in radial direction of the enclosure for different values of Darcy numbers.

5.6. Velocity profile

Figure 10 explains the variation of dimensionless mean velocity distribution in the radial direction along the minor axis of the enclosure for $\varepsilon = 0.8$, $\mathrm{Pr} = 0.7$, $\theta = 0^{o}, 30^{o}, 60^{o}, 90^{o}$, $\mathrm{Gr} = 10^{6}$, $\mathrm{Da} = 10^{-3}$, $\mathrm{Ha} = 25$

It is observed from the graph that average velocity increases rapidly in the radial direction along the minor axis of the elliptic enclosure from 0 to 0.1 and it becomes uniform in the range of $0.1 \leq R \leq 0.4$ in the radial direction along the minor axis of the enclosure, an indication that there is a limit to have a flow favorable for maximum heat transfer.

Beyond this range, the field flow becomes oscillatory (flow not significant or unsteady) as a result of strong mixing at the core of the enclosure due to the presence of cold and hot fluids where the mean velocity reaches the maximum value along the minor axis of the elliptic enclosure

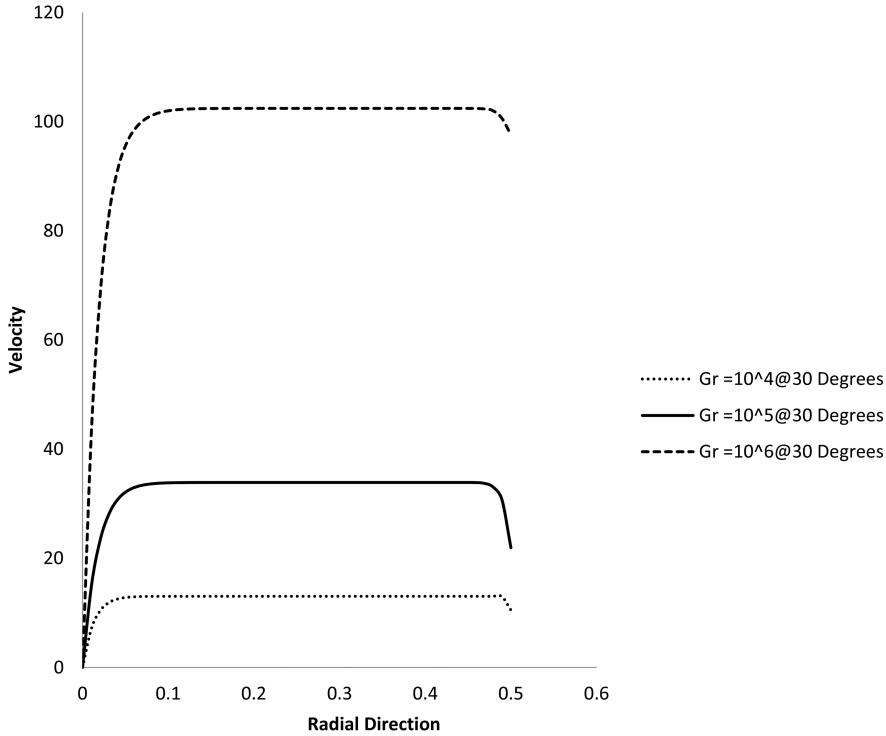

Fig. 9. Velocity distribution in radial direction of the enclosure for different values of Grashof numbers.

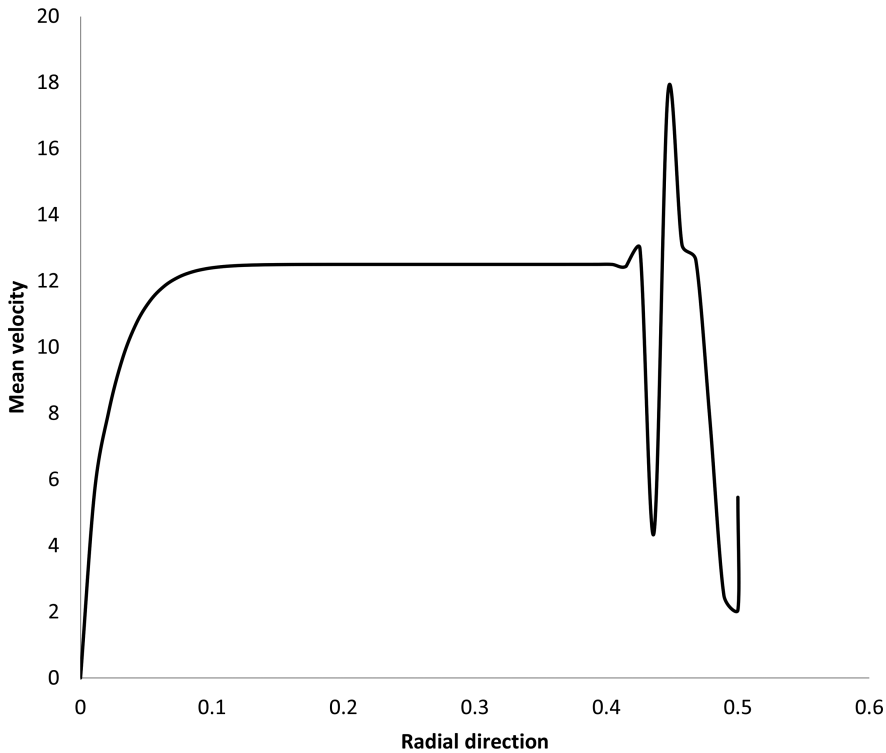

Fig. 10. Velocity profile of the flow in the enclosure.

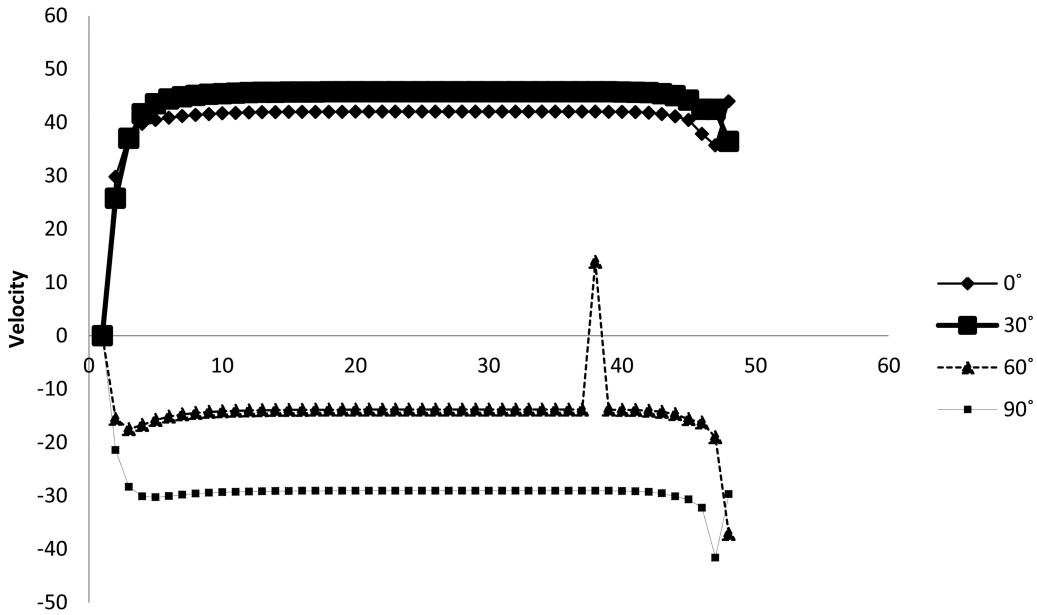

Fig. 11. Angle of inclination.

5.7. Effect of enclosure inclination angle on flow circulation (velocity distribution)

Figure 11 illustrates the variation of velocity distribution (flow circulation) with respect to different enclosure inclination angles ($\theta = 0^o, 30^o, 60^o, 90^o$) for $\varepsilon = 0.8$, Pr = 0.7, Gr = 10^6, Ha = 25, and Da = 10^{-3}. It is observed from the plot that the strength of the flow circulation decreases as the enclosure inclination angle increases from $\theta = 30^o$ to $\theta = 90^o$.

6. Conclusions

The geometric parameters and fluid properties were varied under the following conditions, Ha = 25, Gr = 10^6, e = 0.8, $\theta = 30^o$, Da = 10^{-3}, Pr = 0.7. From the study, the following conclusions were drawn

- The numerical results obtained from the study were compared with the published related geometries by comparing their average Nusselt numbers (i.e., the rate of heat transfer) which includes the following: Tilted elliptic cylinder with no deviation (0%), elliptic duct with no deviation (0%), horizontal elliptic duct with no deviation (0%), inclined elliptic enclosure with (5.49%) deviation, circular and cylindrical enclosure with (1.62%) deviation, circular enclosure with (11.8%) deviation, circular and elliptic enclosure with (0.92%) deviation and elliptic duct with (0.866%).

- The result obtained from the study indicated that the Nusselt numbers at the end of minor axis is greater than the major axis (minor, Nu = 4.2 and major, Nu = 3.0).

- A critical eccentricity, $e = 0.8$ is attained for optimum heat transfer by convection.

- The difference between the heat transfer rate at the end of major and minor axis of the configuration within the parametric range $0 \leq e \leq 0.2$ is insignificant (Nu = 3.24 and Nu = 3.25).

- Above $e = 0.2$, more heat is transferred from the end of the minor axis of the enclosure. It is also observed from the plot that the higher the value of eccentricity, e, the higher the rate of heat transfer between the parametric range considered, that is, $0.4 \leq e \leq 0.8$ but decreases within the parametric range $180^0 \leq \Phi \leq 270^0$.

- The effect of Hartmann number on flow circulation(velocity distribution) of the enclosure for Ha = 0, 25 and 50 are 80, 60 and 58 (i.e., Hartmann number increased with decreased flow circulation)

- The effect of angle of inclination on heat transfer rate is significant from 58^0 to 90^0.

- A strong flow circulation (velocity distribution) is obtained when $Gr = 10^6$ and $Da = 10^{-4}$.

- The study established that the geometry and fluid properties influence the flow circulation and heat transfer characteristics in the elliptic configuration considered.

Literature Cited

1. Bhuiyan AH, Uddin MN, Alim MA. Combined effect of Hartmann and Raleigh numbers on free convection flow in a square cavity with different positions of heat elliptic obstacle. Annal Pure Appl Math 2014;41–56.
2. Hussein AK, et al. MHD natural convection inside inclined trapezoida enclosure with internal heat generation or absorption subjected to isoflux heating. Int Heat Transf-Asian Res 2012 DOI 10.1002/htj.210134.
3. Hojjat HN, Hmid N, Seyyed AM. CFD analysis of laminar natural convection from horizontal circular cylinder to its contric elliptic enclosure. 15th Conference on Fluid Dynamic (2013) December 18–20, University of Hormozgan Bandar Abbas,Iraq.
4. Moghimi, G., Domairry SM, Bararmia H, Soheil S, Ghasemi E. Numerical study of natural convection in an inclined L-shaped porous enclosure. Adv Theor Appl Mech 2012;5:237–245.
5. Cho YH. Effect of a magnetic field on natural convection of an electrically conducting fluid in a tilted cavity. J Phys Soc 2009;55:2193–2199.
6. Tsetkov P, Shoaib U, Steven K ed. Nuclear energy encyclopedia; science. Technology and Application, Hboken, Wiley, 2011;48:85.
7. Bakhshan Y, AShoori H. Analysis of a fluid behavior in a rectangular enclosure under the effect of a magnetic field 2012;61.
8. Oreper GM, Szekely J. The effect of an externally imposed magnetic Fieldon buoyancy driven flow in a rectangular cavity. J Cryst Growth 1983;64:505.
9. Shah RK, London AL. Laminar flow forced convection in ducts. Academic Press, New York; 1978. (Chapter ix, pp. 247–252, Chapter 11, p. 7).
10. Akel AM. Natural convection with uniformly heated inner elliptic cylinder and outer square cylinder. Engr Technol J 2012;30:19.
11. Mota JPB, et al. Natural convection heat transfer in horizontal eccentric elliptic annuli containing saturated porous media. Int J Mass Heat Transf 2000;43:4367–4379.
12. Kakas S, Shah RK, Aung W. Handbook of single phase convective heat and mass transfer. Wiley, New York; 1988. p 63–68.

13. Eid EI. Natural convection heat transfer in elliptic in annuli with different aspect ratios. Alexandria Engr J 2005;44:203–215.
14. Sakalis VD, Hatzikonstantinon PM, Kafonsias N. Thermally developing flow in elliptic duct with axially variable wall temperature distribution. Int J Heat Mass Transf 2002;45:25–35.
15. Abdel-Wahed RM, Attia AE, Hifni MA. Experiments on laminar flow and heat transfer in an elliptic duct. Int J Heat Mass Transf 1984;27:2397–2411.
16. Mahfouz FM. Buoyancy driven flow within an inclined elliptic enclosure. Int J Thermal Sci 2011;50:1887–1899.
17. Ghasemi E, Soleimani S, Bararnia H. Natural convection in a circular and elliptical cylinder enclosure. Int J Commun Heat Mass Transf 2012;39:1035–1044.
18. Bello-Ochende FL, Adegun IK. A perturbation analysis of combined free and forced laminar convection in tilted elliptic cylinder. Sixth Int Symposium on Transport Phenomenoa in Thermal Engineering. Seuol, Korea. 1993;3:121–125.
19. Adegun IK, Oladosu OA. Scale analysis of free and forced fluid flow convective heat transfer in the entrance region of elliptic conduits. New York Sci J 2009; ISSN 1554–0200.
20. Fatih S, Hakan FO. Numerical study of MHD mixed convection in a nanofluid filled lid driven square enclosure with a rotating cylinder. Int J Heat Mass Transf 2014;78:741–754.
21. Fatih S, Hakan FO. MHD mixed convection of nanofluid filled partially heated triangular enclosure with a rotating adiabatic cylinder. J Taiwan Inst Chem Engr 2014.
22. Fatih S, Hakan FO. Natural convection and entropy generation of nanofluid filled cavity having diffent shaped obstacles under the influence of magnetic field and internal heat generation 2015;56:42–56.
23. Fatih S, Hakan FO. Influence of inclination angle of magnetic field on mixed convection of nanofluid flow over a backward facing step and entropy generation. Adv Power Technol 2015.
24. Istrael-Cookey C, Amos E, Nwaigna C. MHD oscillatory couette of a radiating viscous fluid in a porous media with periodic wall temperature. Am J Scientif Int Res 2010;326–331.
25. Ahmed WM. Natural convection in parabolic enclosure heated from below. Modern Appl Sci 2011;5.
26. Moghimi SM, et al. Numerical study of natural convection in an inclined L-shaped porous enclosure. Adv Theor Appl Mech 2012;5:237–245.
27. Habibis S, Sri S, Isak H. Computation of natural convection in a porous parallelogrammic enclosure with magnetic field. MAKARA, SAINS 2010;4:188–199.
28. Hakan FO, Eiyad AN, Yasir V. Numerical convection in wavy enclosure with volumetric heat source. Int J Thermal Sci 2011;50:502–514.
29. Verzicco R, Orlandi P. A finite difference scheme for three-dimensional incompressible flow in cylindrical coordinates. J Computat Phys, Elsevier 2002;123:402–414.
30. Necati O. Finite difference method in heat transfer, CRC Press; 1994.
31. Haji-Sheikf A, Vafai K. Analysis of fluid and heat transfer in porous media imbedded inside various-shaped duct. Int J Heat Mass Transf 2004;47:1889–1905.

□♦ ♦ ♦□